ENTROPY GENERATION OF ZIRCONIA-WATER NANOFLUID FLOW THROUGH RECTANGULAR MICRO-CHANNEL

by

Cuneyt UYSAL[a*], Kamil ARSLAN[b], and Huseyin KURT[c]

[a] Automotive Technologies Program, Karabuk University, Karabuk, Turkey
[b] Mechanical Engineering Department, Karabuk University, Karabuk, Turkey
[c] Mechanical Engineering Department, Necmettin Erbakan University, Konya, Turkey

Original scientific paper
https://doi.org/10.2298/TSCI18S5395U

The fluid flow and heat transfer characteristics and entropy generation of zirconia, ZrO_2-water, nanofluid flow through a rectangular micro-channel are numerically investigated. The flow is considered under single-phase 3-D steady-state incompressible laminar flow conditions. The constant heat flux is applied to the bottom surface of micro-channel. The finite volume method is used to discretize the governing equations. As a result, the average Nusselt number decreases with increasing nanoparticle volume fraction, while the average Darcy friction factor is not affected. Moreover, the total entropy generation decreases with increase in nanoparticle volume fraction, while the Bejan number is almost not affected.

Key words: *Bejan number, entropy generation, nanofluid, Nusselt number, micro-channel*

Introduction

Entropy is the measure of molecular disorder and randomness. Entropy generation analysis is based on the Second law of thermodynamics and provides accurate performance assessment of any thermodynamic system. Entropy generation analysis also informs about the irreversibilities due to flow friction and heat transfer through a finite temperature difference, mixing, chemical reactions, *etc*. [1].

The nanofluid term was introduced by Choi and Eastman [2]. Nanofluids are prepared with metallic or non-metallic nanoparticle addition to conventional working fluids such as water, ethylene glycol or lubricants to obtain working fluids having better thermophysical properties. Nanofluids can be used as heat transfer fluid in internal combustion engines [3-6], solar collectors [7-11], building heating and cooling systems [12-14], nuclear reactors [15-17], electronic components [18-20], and many more in practice.

The entropy generation due to fluid friction and heat transfer of some nanofluids under different conditions have been studied in [21-24]. Singh *et al.* [25] investigated the effect of tube diameter on entropy generation of Al_2O_3-water nanofluid flow. They observed that the flow friction irreversibility is dominant at lower tube diameter, while heat transfer irreversibility is dominant at higher tube diameter. Also, optimum diameter was defined to minimize entropy generation for a given nanofluid. Mah *et al.* [26] showed that the entropy generation

* Corresponding author, e-mail: cuneytuysal@karabuk.edu.tr

significantly increases when the viscous dissipation effect is taken into account for fully developed forced convection of Al_2O_3-water nanofluid flow through circular micro-channels. Ting *et al.* [27] investigated the entropy generation of Al_2O_3-water nanofluid flow in asymmetrically heated porous micro-channel with solid-phase heat generation. It was reported that entropy generation decreases with decrease in internal heat generation. It was also found that the entropy generation can be reduced as much as 42%, when the suspended nanoparticle is smaller than threshold size. Rashidi *et al.* [28] derived a mathematical formulation to calculate entropy generation of Cu-water, CuO-water, and Al_2O_3-water nanofluid flow over a rotating porous disk under MHD effect. Rashidi *et al.* [29] used homotopy analysis method, artificial neural network, and particle swarm optimization to minimize entropy generation for flows over a rotating disk under uniform vertical magnetic field. Rashidi *et al.* [30] studied the change of entropy generation and Bejan number with magnetic interaction number for flows over a rotating disk. Sheikholeslami *et al.* [31] investigated the forced convection heat transfer in a lid driven semi annulus enclosure filled with Fe_3O_4-water nanofluid under non-uniform magnetic field. It was reported that Nusselt number is directly proportional with Reynolds number and nanoparticle volume fraction, while it is inversely proportional with Hartmann number.

Limited studies exist in the literature about thermal and hydrodynamic performance of ZrO_2-water nanofluid flow. Goharshadi and Hadadian [32] investigated the rheological properties of ZrO_2-ethylene glycol nanofluids. Haghighi *et al.* [33] studied the thermal conductivity and single phase laminar convective heat transfer of Al_2O_3-water, ZrO_2-water, and TiO_2-water nanofluids in a microtube. Haghighi *et al.* [34] also investigated the convective heat transfer coefficient of Al_2O_3-water, ZrO_2-water, and TiO_2-water nanofluid inside straight tube under both laminar and turbulent regime. They found that maximum convective heat transfer enhancement is obtained to be 23% for Al_2O_3-water nanofluid and followed by ZrO_2-water and TiO_2-water nanofluids with 15% and 8%, respectively. Purohit *et al.* [35] studied the laminar forced convective heat transfer of ZrO_2-water and TiO_2-water nanofluid flow. It was reported that the entropy generation slightly decreases with nanoparticle addition to base fluid under same Reynolds number.

In this study, the entropy generation and laminar convective heat transfer characteristics of ZrO_2-water nanofluid through a rectangular micro-channel have been numerically investigated. In the analysis, different nanoparticle volume fractions of ZrO_2-water nanofluid are used. Constant heat flux of 1000 W/m^2 is applied to the bottom surface of micro-channel. The convective heat transfer coefficient, Nusselt number, pressure drop, Darcy friction factor, entropy generation, and Bejan number have been determined.

Mathematical modelling

Micro-channels are used for cooling of electronic devices in practice. In this study, a rectangular micro-channel is modeled to analyze. The hydraulic diameter and length of rectangular micro-channel are defined to be 150 μm and 5 cm, respectively. The aspect ratio ($\alpha = H/W$) of micro-channel is defined to be 1.6 and height, H, and width, W, of micro-channel are calculated by:

$$D_h = \frac{4A}{P} = \frac{2HW}{H+W} \tag{1}$$

The dimensions of rectangular micro-channel are given in tab. 1.

Table 1. Dimensions of rectangular micro-channel

$\alpha = H/W$	D_h [μm]	L [cm]	H [μm]	W [μm]
1.6	150	5	195	121.875

In the mathematical modeling of single-phase steady-state incompressible laminar flow, the following governing equations are used:

$$\mathrm{div}(\rho\vec{\mathrm{V}}) = 0 \tag{2}$$

$$\mathrm{div}(\rho\vec{\mathrm{V}}\vec{\mathrm{V}}) = -\mathrm{grad}\,P + \mathrm{div}(\mu\,\mathrm{grad}\,\vec{\mathrm{V}}) \tag{3}$$

$$\mathrm{div}(\rho C_P\vec{\mathrm{V}}T) = \mathrm{div}(k\,\mathrm{grad}\,T) \tag{4}$$

In the governing equations, viscous dissipation, and radiation heat transfer are assumed to be negligible. In addition, natural convection effect is neglected since lower value of Richardson number compared with Ri = 0.1. Constant inlet velocity is applied, and the inlet velocity can be calculated *via* specified Reynolds number:

$$U_{\mathrm{inlet}} = \frac{\mu_{\mathrm{nf}}\,\mathrm{Re}}{\rho_{\mathrm{nf}}\,D_h} \tag{5}$$

where μ_{nf} [Pa·s] is the viscosity and ρ_{nf} [kgm^{-3}] – the density. The pressure outlet boundary condition is also applied. Constant heat flux of 1000 W/m^2 is applied to the bottom wall of rectangular micro-channel.

To solve the governing equations, the thermophysical properties of working fluid existing in the governing equations should be defined. The density and specific heat of ZrO_2-water nanofluid can be defined with following equations which are based on conventional mixture theory [36], respectively:

$$\rho_{\mathrm{nf}} = \varphi\rho_{\mathrm{np}} + (1-\varphi)\rho_{\mathrm{bf}} \tag{6}$$

$$(\rho C_P)_{\mathrm{nf}} = \varphi(\rho C_P)_{\mathrm{np}} + (1-\varphi)(\rho C_P)_{\mathrm{bf}} \tag{7}$$

where φ is the nanoparticle volume fraction and C_P [Jkg^{-1}K^{-1}] – the specific heat. The subscripts nf, np, and bf denote the nanofluid, nanoparticle, and base fluid, respectively.

The thermal conductivity of ZrO_2-water nanofluid can be calculated by the following equation proposed by Hamilton and Crosser [37]:

$$k_{\mathrm{nf}} = \left[\frac{k_{\mathrm{np}} + (n-1)k_{\mathrm{bf}} - (n-1)(k_{\mathrm{bf}} - k_{\mathrm{np}})\varphi}{k_{\mathrm{np}} + (n-1)k_{\mathrm{bf}} + (k_{\mathrm{bf}} - k_{\mathrm{np}})\varphi}\right]k_{\mathrm{bf}} \tag{8}$$

where k is the thermal conductivity coefficient and n – the nanoparticle shape factor and can be taken as 3 for spherical nanoparticles.

The viscosity of ZrO_2-water nanofluid can be found by the following equation proposed by de Brujin [38] which is extended of Einstein model and applicable for spherical nanoparticles and high nanoparticle volume fractions:

$$\mu_{\mathrm{nf}} = \left[\frac{1}{1-2.5\varphi+1.552\varphi^2}\right]\mu_{\mathrm{bf}} \tag{9}$$

The thermophysical properties for base fluid and nanoparticle which are required to calculate the thermophysical properties of nanofluid are given in tab. 2.

Table 2. Thermophysical properties for base fluid and nanoparticle [35, 39]

Material	ρ [kgm^{-3}]	C_P [Jkg^{-1}K^{-1}]	k [Wm^{-1}K^{-1}]	μ [Pa·s]
Water	993.05	4178	0.628	0.000695
Zirconia	5600	418	2.8	–

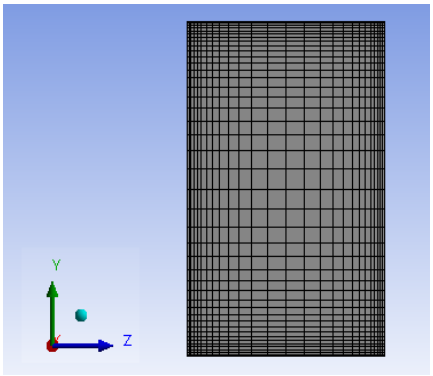

Figure 1. The mesh distribution of rectangular micro-channel

Table 3. Mesh independency test

Mesh	Nu	f	ΔNu [%]	Δf [%]
4720	3.5527	0.05277	–	–
49600	3.7783	0.06101	6.35	15.6
144000	3.8085	0.06262	0.8	2.65
264654	3.8207	0.06296	0.32	0.53
465080	3.8268	0.06323	0.16	0.44
659568	3.8268	0.06339	0	0.25

Hexahedral mesh distribution is used in the modeling of rectangular micro-channel. Finer meshes are used in the near regions to walls and corners of rectangular micro-channel to provide more accurate solution. The mesh distribution of rectangular micro-channel is shown in fig. 1.

Finite volume method is used to carry out the numerical computation. The governing equations are solved with boundary conditions. The SIMPLE algorithm is used to resolve velocity and pressure coupling [40]. In this method, the computational domain is divided into a number of cells. The location of the velocity components are at the center of the cell faces to which they are normal. The discretized form of continuity equation is obtained with applying finite volume method. Axial and transverse fluxes of momentum equation are found. To obtain the provisional values of velocity components, momentum equations are solved. Then making use of the approximate velocity solution, a pressure correction is evolved and also a velocity correction is obtained. Velocity and pressure corrections are linked. The advantage of this method is that transport rates across the faces of the control volumes can be computed without interpolation of velocity components. To discretize the momentum and energy equation, Green Gauss cell-based method is used. The convergence criterion of 10^{-6} is used in the iteration of governing equations. The CPU time is obtained to be approximately 225.67 seconds for the analyses.

Mesh independency test is carried out to make ineffective the effect of grid number on the results. Various grids are tested and the changes of average Nusselt number and average Darcy friction factor are obtained. The results are shown in tab. 3. To carry out the solutions, the model having 659568 grid numbers is selected as optimum mesh number.

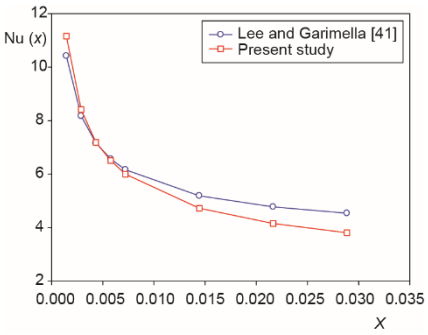

Figure 2. The model accuracy test

To test accuracy and consistency of selected model, the local Nusselt number values obtained from numerical solution of base fluid are compared with the correlation proposed for thermally developing flow in rectangular micro-channel by Lee and Garimella [41]. The comparison of results obtained by present study with that of Lee and Garimella is illustrated in fig. 2. As can be seen from fig. 2, the results obtained by the present study show good agreement with the results obtained by Lee and Garimella.

The dimensionless distance used in fig. 2 is expressed:

$$X = \frac{x}{\mathrm{Re}\,\mathrm{Pr}\,D_\mathrm{h}} \tag{10}$$

where x [m] is axial distance and Pr – the Prandtl number. Local Nusselt number is defined by:

$$\mathrm{Nu}(x) = \frac{h(x)D_\mathrm{h}}{k_\mathrm{nf}} \tag{11}$$

where $h(x)$ is the local convective heat transfer and is expressed:

$$h(x) = \frac{q''}{T_\mathrm{w}(x) - T_\mathrm{b}(x)} \tag{12}$$

where q'' [Wm^{-2}] is the heat flux, $T_\mathrm{w}(x)$ [K] and $T_\mathrm{b}(x)$ [K] are local wall temperature and local bulk temperature, respectively.

The average convective heat transfer coefficient and average Nusselt number are calculated by following equations, respectively:

$$h = \frac{1}{L}\int_0^L h(x)\mathrm{d}x \tag{13}$$

$$\mathrm{Nu} = \frac{1}{L}\int_0^L \mathrm{Nu}(x)\mathrm{d}x \tag{14}$$

The average Darcy friction factor is calculated by:

$$f = 2\frac{D_\mathrm{h}}{L}\frac{\Delta P}{\rho_\mathrm{nf}U^2} \tag{15}$$

where ΔP [Pa] is the pressure drop along the micro-channel and U [ms^{-1}] – the velocity of working fluid.

The entropy generation per unit length for internal flow can be written [1]:

$$\dot{S}'_\mathrm{gen} = \dot{S}'_\mathrm{gen,\,heat\,transfer} + \dot{S}'_\mathrm{gen,\,fluid\,friction} \tag{16}$$

where $\dot{S}'_{\text{gen, heat transfer}}$ is defined as $(q''^2\pi D_h^2)/(k_{nf}T_b^2\,\text{Nu})$, while $\dot{S}'_{\text{gen, fluid friction}}$ is expressed as $(8\dot{m}^3 f)/(\pi^2\rho_{nf}{}^2T_bD_h^5)$. The Bejan number can be written in the context of thermodynamics:

$$\text{Be} = \frac{\dot{S}'_{\text{gen, heat transfer}}}{\dot{S}'_{\text{gen, heat transfer}} + \dot{S}'_{\text{gen, fluid friction}}} \tag{17}$$

where $\dot{S}'_{\text{gen}}$ [$\text{Wm}^{-1}\text{K}^{-1}$] is the entropy generation per unit length. Bejan number is defined as the ratio of heat transfer irreversibility to total irreversibility due to heat transfer and fluid friction.

Results and discussion

The fluid flow and heat transfer characteristics and entropy generation of ZrO_2-water nanofluid flow through a rectangular micro-channel is numerically investigated. The flow is considered under single-phase, 3-D thermally developing incompressible steady-state laminar flow conditions. Reynolds number considered in this study is in the range of 100 and 1000. Constant heat flux of q'' = 1000 W/m^2 is applied to the bottom surface of rectangular micro--channel.

The variation of convective heat transfer coefficient with the Reynolds number for different nanoparticle volume fractions is illustrated in fig. 3. As can be seen from fig. 3, the convective heat transfer coefficient increases with increase in nanoparticle volume fraction of ZrO_2-water nanofluid and Reynolds number. The convective heat transfer enhancements for 4.0% ZrO_2-water nanofluid at Re = 100 and Re = 1000 are obtained to be 4.37% and 2.3% compared to pure water, respectively. Zirconia nanoparticles adding into the pure water deform the boundary-layer near to the wall of the micro-channel. Consequently, the convective heat transfer increases by this effect. Also, increasing nanoparticle volume fraction increases the deformation of the boundary-layer and convective heat transfer.

The variation of Nusselt number with the Reynolds number is shown in fig. 4. The Nusselt number decreases with increase in nanoparticle volume fraction of ZrO_2-water nanofluid. The Nusselt number values obtained for 4.0% ZrO_2-water at Re = 100 and Re = 1000 are 2.05% and 3.99% lower compared to that of pure water. In the calculations, it is observed that thermal conductivity coefficient increases 6.56 % when ZrO_2 nanoparticle addition of 4.0% to pure water. However, the maximum enhancement in convective heat

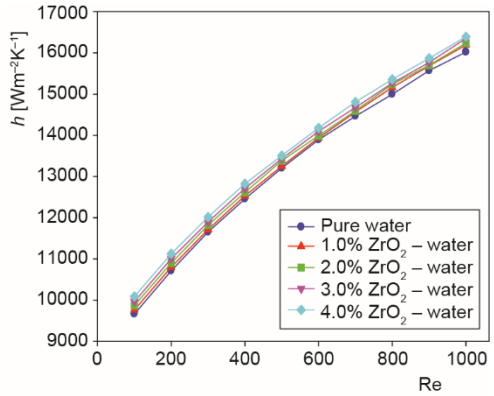

Figure 3. Variation of convective heat transfer coefficient with the Reynolds number

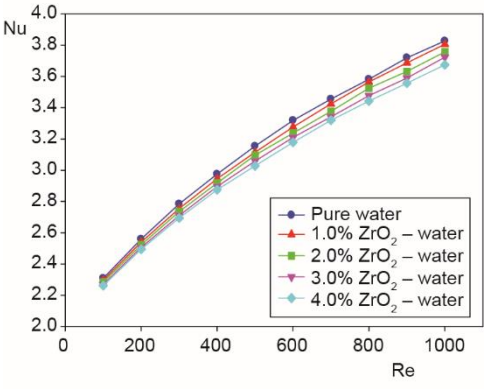

Figure 4. Variation of Nusselt number with the Reynolds number

transfer coefficient is obtained to be 4.37%. Higher enhancement in thermal conductivity coefficient compared to convective heat transfer coefficient reduces the Nusselt number.

The variation of pressure drop with the Reynolds number for different nanoparticle volume fractions is illustrated in fig. 5. As can be seen from fig. 5, the pressure drop increases with increase in nanoparticle volume fraction of ZrO_2-water nanofluid. The pressure drops for 4.0% ZrO_2-water nanofluid at Re = 100 and Re = 1000 are 3.53% and 3.54% higher compared to that of pure water, respectively. Adding the zirconia nanoparticles into the pure water increase the viscosity of the nanofluid progressively. This effect increases the pressure drop since the pressure drop into the micro-channel depends mostly on viscosity of the working fluid.

The variation of Darcy friction factor with the Reynolds number is illustrated in fig. 6. It is observed that ZrO_2 nanoparticle addition to pure water does not affect the Darcy friction factor of flow. Increasing volume fraction of the nanofluid increases the pressure drop into the micro-channel. However, this increment has no effect on Darcy friction factor. In addition, increase of the pressure drop is nearly close to the value of the increment of the density of nanofluid. Hence, the Darcy friction factor is not affected by the increasing of volume fraction of nanofluid.

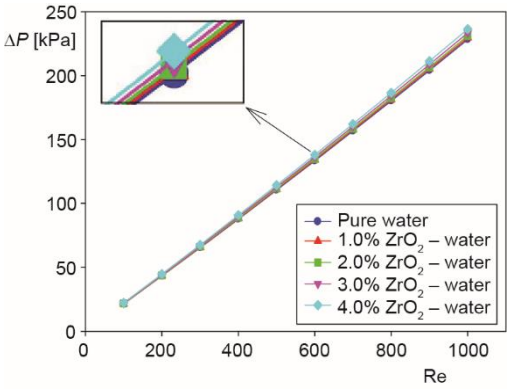

Figure 5. Variation of pressure drop with the Reynolds number

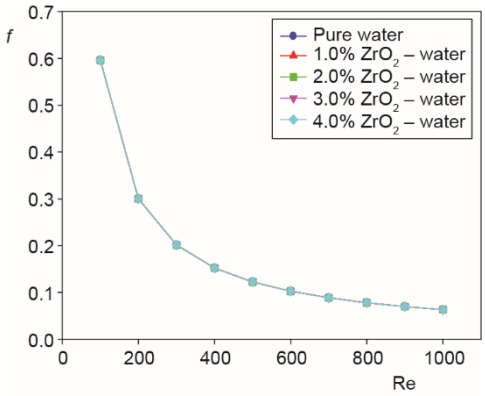

Figure 6. Variation of Darcy friction factor with the Reynolds number

Figure 7 shows the variation of entropy generation due to heat transfer with the Reynolds number. As can be seen from fig. 7, the entropy generation due to heat transfer decreases with increase in Reynolds number or nanoparticle volume fraction of nanofluid. The entropy generations due to heat transfer obtained for 4.0% ZrO_2-water nanofluid at Re = 100 and Re = 1000 are 4.19% and 2.25% lower compared to that of pure water, respectively. This decrement in entropy generation due to heat transfer is due to bulk temperature and convective heat transfer increase with increasing nanoparticle volume fraction of ZrO_2-water nanofluid. Also, increasing the Reynolds number increases the Nusselt number and decreases the bulk temperature. Increment in Nusselt number is higher compared to decrement in the bulk temperature. Therefore, entropy generation due to heat transfer decreases with increase in Reynolds number.

The variation of entropy generation due to fluid friction with the Reynolds number is illustrated in fig. 8. It is observed that entropy generation due to fluid friction increases with increasing Reynolds number while it decreases with increasing nanoparticle volume fraction

of ZrO_2-water nanofluid. The entropy generations due to fluid friction obtained for 4.0% ZrO_2-water nanofluid at Re = 100 and Re = 1000 are 3.25% and 3.24% lower than that of pure water, respectively. The source of reduction in entropy generation due to fluid friction results from that the ZrO_2 nanoparticle addition to pure water leads to increase in bulk temperature. The analyses are performed on defined Reynolds number values. The ZrO_2 nanoparticle addition to pure water leads to increase in velocity to provide defined Reynolds number value. Although the density and velocity increase with ZrO_2 nanoparticle addition to pure water, the entropy generation due to fluid friction decreases with increasing nanoparticle volume fraction of ZrO_2-water nanofluid. This is because increment in bulk temperature is higher than that of velocity and density.

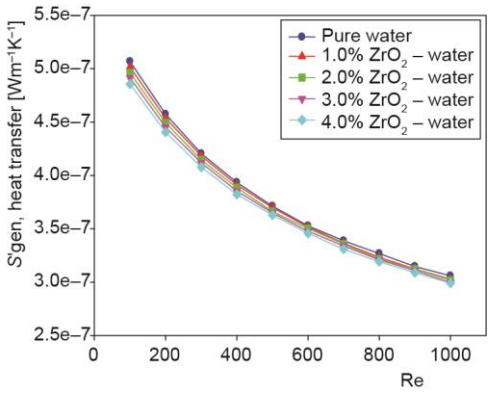

Figure 7. Variation of entropy generation due to heat transfer with the Reynolds number

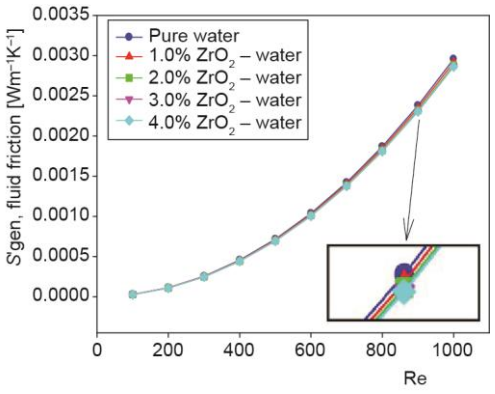

Figure 8. Variation of entropy generation due to fluid friction with the Reynolds number

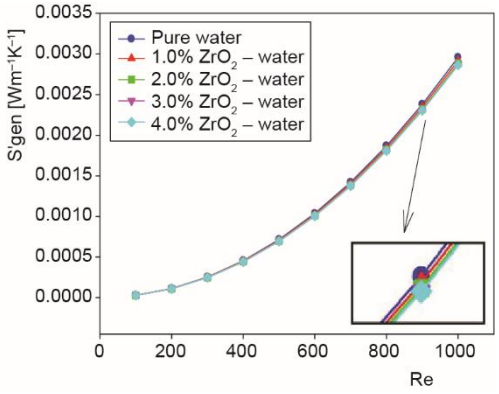

Figure 9. Variation of total entropy generation with the Reynolds number

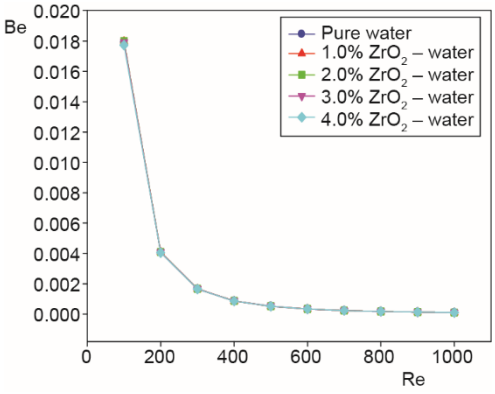

Figure 10. Variation of Bejan number with the Reynolds number

Figure 9 shows that the variation of total entropy generation with Reynolds number. It is observed that total entropy generation due to heat transfer and fluid friction decreases with increase in nanoparticle volume fraction of ZrO_2-water nanofluid. The total entropy generation obtained for 4.0% ZrO_2-water nanofluid at Re = 100 and Re = 1000 are 3.27% and 3.24% lower than that of pure water, respectively. It is also observed that the entropy genera-

tion due to fluid flow is dominant for flow through micro-channel. This fact is compatible with the results of Singh *et al.* [25].

The variation of the Bejan number with the Reynolds number is illustrated in fig. 10. It is observed that the Bejan number decreases with increase in Reynolds number. Moreover, the Bejan number is not almost affected by the ZrO_2 nanoparticle addition to pure water.

Conclusions

The fluid-flow and heat transfer characteristics and entropy generation of ZrO_2-water nanofluid flow through a rectangular micro-channel are numerically investigated under single-phase steady-state laminar flow conditions. The convective heat transfer coefficient increases with increasing nanoparticle volume fraction of ZrO_2-water nanofluid. However, this increment is not higher than 4.37% compared to pure water for whole study because of that the ZrO_2 has low thermal conductivity coefficient. Contrary to convective heat transfer, Nusselt number decreases with increase in nanoparticle volume fraction of ZrO_2-water nanofluid. It is due to that increment in thermal conductivity coefficient is higher than that of convective heat transfer when ZrO_2 nanoparticle added to pure water. The Darcy friction factor is not affected by ZrO_2 nanoparticle addition to pure water, although the pressure drop increases with increasing of nanoparticle volume fraction of ZrO_2-water nanofluid. This means that dimensionless pressure drop does not change with ZrO_2 nanoparticle addition to pure water. The entropy generations due to heat transfer and due to fluid friction decrease with increase in nanoparticle volume fraction of ZrO_2-water nanofluid. It is found that the entropy generation due to fluid friction is dominant. This is due to micro-channels have small hydraulic diameter.

Acknowledgment

This study was supported by Scientific Research Projects Coordination Unit of Karabuk University (Project Number: KBUBAP-17-YD-223).

Nomenclature

A – area, [m^2]
Be – Bejan number
C_P – specific heat, [$Jkg^{-1}K^{-1}$]
D_h – hydraulic diameter, [m]
f – Darcy friction factor
H – height, [m]
h – convective heat transfer coefficient, [$Wm^{-2}K^{-1}$]
k – conductive heat transfer coefficient, [$Wm^{-1}K^{-1}$]
L – length, [m]
$\dot{m}$ – mass-flow rate, [kgs^{-1}]
n – nanoparticle shape particle
Nu – Nusselt number
P – pressure, [Pa]
Pr – Prandtl number
q'' – heat flux, [Wm^{-2}]
Re – Reynolds number
Ri – Richardson number
$\dot{S}'_{gen}$ – entropy generation rate per unit length, [$Wm^{-1}K^{-1}$]
T – temperature, [K]
$\vec{V}$ – velocity vector
W – width, [m]
X – dimensionless distance
x – distance, [m]

Subscripts

b – bulk
bf – base fluid
nf – nanofluid
np – nanoparticle
w – wall
div – divergence
grad – gradient

Greek symbols

μ – dynamic viscosity [Pa·s]
ρ – density [kgm^{-3}]
φ – volumetric fraction [%]

References

[1] Bejan, A., *Entropy Generation through Heat and Fluid Flow*, John Wiley and Sons, New York, 1982
[2] Choi, S. U. S., Eastman, J. A., Enhancing Thermal Conductivity of Fluids with Nanoparticles, *Proceedings*, ASME International Mechanical Engineering Congress and Exposition, San Francisco, Cal., USA, p.p. 1-8, 1995
[3] Moghaieb, H. S., *et al*., Engine Cooling Using Al_2O_3/Water Nanofluids, *Applied Thermal Engineering*, *115* (2017), Mar., pp. 152-159
[4] Tzeng, S. C., *et al*., Heat Transfer Enhancement of Nanofluids in Rotary Blade Coupling of Four-Wheel-Drive Vehicles, *Acta Mechanica*, *179* (2005), 1-2, pp. 11-23
[5] Kole, M., Dey, T. K., Thermal Conductivity and Viscosity of Al_2O_3 Nanofluid Based on Car Engine Coolant, *Journal of Physics D: Applied Physics*, *43* (2010), 31, ID 315501
[6] Chougule, S. S., Sahu, S. K., Comparative Study of Cooling Performance of Automobile Radiator Using Al_2O_3-Water and Carbon Nanotube-Water Nanofluid, *Journal of Nanotechnology in Engineering and Medicine*, *5* (2014), 1, ID 010901
[7] Tyagi, H., *et al*., Predicted Efficiency of a Low-Temperature Nanofluid-Based Direct Absroption Solar Collector, *Solar Energy Engineering*, *131* (2009), 4, ID 0410041-7
[8] Otanicar, T. P., *et al*., Nanofluid-Based Direct Absroption Solar Collector, *Journal of Renewable and Sustainable Energy*, *2* (2010), 3, ID 033102
[9] Yousefi, T., *et al*., An Experimental Investigation on the Effect of Al_2O_3/H_2O Nanofluid on the Efficiency of Flat-Plate Solar Collectors, *Renewable Energy*, *39* (2012), 1, pp. 293-298
[10] Khan, J. A., *et al*., Three-Dimensional Flow of Nanofluid over a Non-Linearly Stretching Sheet: An Application to Solar Energy, *International Journal of Heat and Mass Transfer*, *86* (2015), July, pp. 158-164
[11] Kaya, H., *et al*., Experimental Investigation of Thermal Performance of an Evacuated U-Tube Solar Collector with ZnO-Ethylene Glycol-Pure Water Nanofluids, *Renewable Energy*, *122* (2018), July, pp. 329-338
[12] Rashidi, I., *et al*., Natural Convection of Al_2O_3/Water Nanofluid in a Square Cavity: Effects of Heterogeneous Heating, *International Journal of Heat and Mass Transfer*, *74* (2014), July, pp. 391-402
[13] Said, Z., *et al*., Analysis of Exergy Efficiency and Pumping Power for a Conventional Flat Plate Solar Collector Using SWCNTs Based Nanofluid, *Energy and Buildings*, *78* (2014), Aug., pp. 1-9
[14] Kulkarni, D. P., *et al*., Application of Nanofluids in Heating Buildings and Reducing Pollution, *Applied Energy*, *86* (2009), 12, pp. 2566-2573
[15] Hadad, K., *et al*., Numerical Study of Single and Two-Phase Models of Water/Al_2O_3 Nanofluid Turbulent Forced Convection Flow in VVER-1000 Nuclear Reactor, *Annals of Nuclear Energy*, *60* (2013), Oct., pp. 287-294
[16] Zarifi, E., Jahanfarnia, G., Subchannel Analysis of TiO_2 Nanofluid as the Coolant in VVER-1000 Reactor, *Progress in Nuclear Energy*, *73* (2014), May, pp. 140-152
[17] Hadad, K., *et al*., Nanofluid Application in Post SB-LOCA Transient in VVER-1000 NPP, *Annals of Nuclear Energy*, *79* (2015), May, pp. 101-110
[18] Selvakumar, P., Suresh, S., Convective Performance of CuO/Water Nanofluid in an Electronic Heat Sink, *Experimental Thermal and Fluid Science*, *40* (2012), July, pp. 57-63
[19] Kadri, S., *et al*., A Vertical Magneto-Convection in Square Cavity Containing a Al_2O_3+Water Nanofluid: Cooling of Electronic Compounds, *Energy Procedia*, *18* (2012), 2012, pp. 724-732
[20] Ijam, A., Saidur, R., Nanofluid as a Coolant for Electronic Devices (Cooling of Electronic Devices), *Applied Thermal Engineering*, *32* (2012), Jan., pp. 76-82
[21] Moghaddami, M., *et al*., Second Law Analysis of Nanofluid Flow, *Energy Conversion and Management*, *52* (2011), 2, pp. 1397-1405
[22] Chen, C. K., *et al*., Heat Transfer and Entropy Generation in Fully-Developed Mixed Convection Nanofluid Flow in Vertical Channel, *International Journal of Heat and Mass Transfer*, *79* (2014), Dec., pp. 750-758
[23] Saha, G., Paul, M. C., Analysis of Heat Transfer and Entropy Generation of TiO_2-Water Nanofluid Flow in a Pipe under Transition, *Procedia Engineering*, *105* (2015), 2015, pp. 381-387
[24] Anand, V., Entropy Generation Analysis of Laminar Flow of a Nanofluid in a Circular Tube Immersed in an Isothermal External Fluid, *Energy*, *93* (2015), Part 1, pp. 154-164
[25] Singh, P. K., *et al*., Entropy Generation Due to Flow and Heat Transfer in Nanofluids, *International Journal of Heat and Mass Transfer*, *53* (2010), 21-22, pp. 4757-4767

[26] Mah, W. H., *et al*., Entropy Generation of Viscous Dissipative Nanofluid Flow in Micro-channels, *International Journal of Heat and Mass Transfer*, *55* (2012), 15-16, pp. 4169-4182
[27] Ting, T. W., *et al*., Entropy Generation of Viscous Dissipative Nanofluid Convection in Asymmetrically Heated Porous Micro-channels with Solid-Phase Heat Generation, *Energy Conversion and Management*, *105* (2015), Nov., pp. 731-745
[28] Rashidi, M. M., *et al*., Entropy Generation in Steady MHD Flow Due to a Rotating Porous Disk in a Nanofluid, *International Journal of Heat and Mass Transfer*, *62* (2013), July, pp. 515-525
[29] Rashidi, M. M., *et al*., Parametric Analysis and Optimization of Entropy Generation in Unsteady MHD Flow over a Stretching Rotating Disk Using Artificial Neural Network and Particle Swarm Optimization Algorithm, *Energy*, *55* (2013), June, pp. 497-510
[30] Rashidi, M. M., *et al*., Investigation of Entropy Generation in MHD and Slip Flow over a Rotating Porous Disk with Variable Properties, *International Journal of Heat and Mass Transfer*, *70* (2014), Mar., pp. 892-917
[31] Sheikholeslami, M., *et al*., Effect of Non-Uniform Magnetic Field on Forced Convection Heat Transfer of Fe_3O_4-Water Nanofluid, *Computer Methods in Applied Mechanics and Engineering*, *294* (2015), Sept., pp. 299-312
[32] Goharshadi, E. K., Hadadian, M., Effect of Calcination Temperature on Structural, Vibrational, Optical, and Rheological Properties of Zirconia Nanoparticles, *Ceramics International*, *38* (2012), 3, pp. 771-1777
[33] Haghighi, E. B., *et al*., Screening Single Phase Laminar Convective Heat Transfer of Nanofluids in a Micro-Tube, *Journal of Physics: Conference Series*, *395* (2012), 1, pp. 1-11
[34] Haghighi, E. B., *et al*., Accurate Basis of Comparison for Convective Heat Transfer in Nanofluids, *International Communications in Heat and Mass Transfer*, *52* (2014), Mar., pp. 1-7
[35] Purohit, N., *et al*., Assessment of Nanofluids for Laminar Convective Heat Transfer: A Numerical Study, *Engineering Science and Technology*, *19* (2016), 1, pp. 574-586
[36] Das, S. K., *et al*., *Nanofluids Science and Technology*, John Wiley and Sons, New York, USA, 2008
[37] Hamilton, R. L., Crosser, O. K., Thermal Conductivity of Heterogeneous Two Component Systems, *I&EC Fundamentals*, *1* (1962), 3, pp. 182-191
[38] de Brujin, H., The Viscosity of Suspensions of Spherical Particles, *Recueil des Travaux Chimiques des Pays-Bas*, *61* (1942), 12, pp. 863-874
[39] Incropera, F. P., *et al*., *Introduction to Heat Transfer*, John Wiley and Sons, New York, USA, 2006
[40] Patankar, S. V., *Numerical Heat Transfer and Fluid Flow*, CRC Press, Boka Raton, Fla., USA, 1980
[41] Lee, P. S., Garimella, S. V., Thermally Developing Flow and Heat Transfer in Rectangular Microchannels of Different Aspect Ratios, *International Journal of Heat and Mass Transfer*, *49* (2006), 17-18, pp. 3060-3067

Paper submitted: March 14, 2018
Paper revised: July 24, 2018
Paper accepted: July 26, 2018